Sensing microscopic noise events by frequent quantum measurements

Salvatore Virzì,[1] Laura T. Knoll,[1,2] Alessio Avella,[1] Fabrizio Piacentini,[1,*] Stefano Gherardini,[3] Marco Gramegna,[1] Gershon Kurizki,[4] Abraham G. Kofman,[4] Ivo Pietro Degiovanni,[1,5] Marco Genovese,[1,5] and Filippo Caruso[6]

[1] *Istituto Nazionale di Ricerca Metrologica, Strada delle Cacce 91, Torino 10135, Italy*
[2] *DEILAP-UNIDEF, CITEDEF-CONICET, J. B. de La Salle 4397, 1603 Villa Martelli, Buenos Aires, Argentina*
[3] *Istituto Nazionale di Ottica del Consiglio Nazionale delle Ricerche (CNR-INO), Area Science Park, Basovizza, Trieste 34149, Italy*
[4] *Department of Chemical and Biological Physics, Weizmann Institute of Science, Rehovot 7610001, Israel*
[5] *INFN, sez. di Torino, via P. Giuria 1, Torino 10125, Italy*
[6] *Department of Physics and Astronomy, and European Laboratory for Non-Linear Spectroscopy (LENS), University of Florence, via G. Sansone 1, Sesto Fiorentino 50019, Italy*

(Received 22 December 2022; revised 9 February 2024; accepted 13 February 2024; published 8 March 2024)

We propose and experimentally demonstrate a general method allowing us to unravel microscopic noise events that affect a continuous quantum variable. Such unraveling is achieved by frequent measurements of a discrete variable coupled to the continuous one. The experimental realization involves photons traversing a noisy channel. There, their polarization, whose coupling to the photons' spatial wave packet is subjected to stochastic noise, is frequently measured in the quantum Zeno regime. The measurements not only preserve the polarization state, but also enable the recording of the full noise statistics from the spatially resolved detection of the photons emerging from the channel. This method proves the possibility of employing photons as quantum noise sensors and robust carriers of information.

DOI: 10.1103/PhysRevApplied.21.034014

I. INTRODUCTION

The existing approaches to sensing by quantum probes [1–18] commonly consider the noise [19–26] affecting the probed observables as a nuisance to be suppressed [27]. This can be done either by active dynamical control of the probe [27–30] or (if possible) by confining the sensing to a decoherence-free subspace of the probed object [31–33]. Yet, noise sensing by a quantum probe can be a source of valuable information on the underlying stochastic processes and their detrimental effect on quantum coherence, which is a central obstacle to quantum information technologies [34–43]. Existing noise sensing focuses on noise spectroscopy by qubit probes [44–55], whose dynamical control can enhance their ability to extract noise characteristics, such as the noise memory time [47]. However, all such methods are sensitive only to statistical averages over many noise realizations, and restricted by two major assumptions that severely limit their applicability [27]: (i) the noise is a stationary process (which is often untrue); and (ii) the probe and the bath, which is the source of noise, remain uncorrelated, and the bath state is unchanged by their interaction, i.e., the Born approximation holds.

Here we venture into the scarcely explored domain of *probing individual microscopic noise events* without the restrictions of noise stationarity and the Born approximation. To this end, we resort to *frequent projective measurements* of the probe at intervals that are shorter than (or comparable to) those of noise events. As demonstrated here both theoretically and experimentally, such measurements allow the unraveling of the full statistics of individual noise events, thus providing information impossible to obtain with existing noise sensing methods.

Frequent measurements have been employed to slow down the evolution of quantum systems coupled to baths, thus protecting them from relaxation or decoherence when the measurement rate conforms to the quantum Zeno effect (QZE) [27,49,56–66]. We have recently demonstrated [67] that polarization measurements of a photonic probe can disclose the sign of correlations between consecutive polarization fluctuations in a noisy medium (bath) that adheres to the Born approximation.

Here we consider a different and far more general scenario, where *the probe (system) and the bath become entangled* by each noise event (inducing decoherence on the system state), and the probe measurements keep changing the (continuous-variable) bath state. An appropriate probe-measurement rate conforming to the QZE is shown

*f.piacentini@inrim.it

to reveal the distribution of random probe-bath couplings, particularly, the second moment of the distribution. This hitherto unavailable information can be used to devise unexplored strategies of noise sensing and control.

II. THEORETICAL FRAMEWORK

A. Sensing bath-induced noise by frequent probe measurements

Consider a quantum system coupled to a bath via the interaction Hamiltonian

$$H_{\rm I} = -\kappa(t) S \otimes B, \tag{1}$$

where S and B are the operators of the system (S) and the bath (B), respectively, $\kappa(t)$ is the time-dependent (here stochastic) coupling strength, and we assume that the Hamiltonian of both S and B vanishes.

The combined *supersystem* (S + B) evolves via the unitary operator $U(t) = e^{iG(t)S\otimes B}$, where $G(t) = \int_0^t d\tau\, \kappa(\tau)$. Let the initial state of the supersystem be $|\Psi_{\rm in}\rangle = |\psi\rangle \otimes |f\rangle$, where $|\psi\rangle$ and $|f\rangle$ are the initial states of S and B, respectively. The probability that S will remain in its initial state is given by $p(t) = {\rm Tr}(\Pi_\psi |\Psi(t)\rangle\langle\Psi(t)|)$, where $\Pi_\psi = |\psi\rangle\langle\psi|$ and $|\Psi(t)\rangle = U(t)|\Psi_{\rm in}\rangle$. For sufficiently small t, we can expand the exponential in $U(t)$ up to second order, yielding

$$p(t) = 1 - G^2(t)\Delta S^2\, \overline{B^2}, \tag{2}$$

where $\overline{B^2} = \langle f|B^2|f\rangle$, $\overline{S^n} = \langle\psi|S^n|\psi\rangle$, and $\Delta S^2 = \overline{S^2} - \overline{S}^2$ is the variance of S in the state $|\psi\rangle$. Assume that the system S is measured in the state $|\psi\rangle$ at *random* instants t_j in the time interval $[0, T]$ and, immediately after each t_j ($j = 1, \ldots, N$; $t_N = T$), it is coupled to a new bath in the same state $|f\rangle$. If the intervals $\tau_j = t_j - t_{j-1}$ (where $t_0 = 0$) are sufficiently short, then the total survival probability of the system state $|\psi\rangle$ is a product of expressions of the form of Eq. (2), yielding

$$p_{\rm tot} = e^{-J_N}, \quad J_N = \Delta S^2\, \overline{B^2} \sum_{j=1}^{N} g_j^2, \tag{3}$$

where $g_j = \int_{t_{j-1}}^{t_j} dt\, \kappa(t)$.

Essentially, we treat the effective coupling g_j as random. To this end, t_j can be either random or regular, as long as $\kappa(t)$ is random.

For simplicity, we assume that the stochastic $\kappa(t)$ does not change sign, i.e., $\kappa(t) \geq 0$. Consider first the effect of unitary evolution, so that there is only one measurement at the end of the process, at $t_1 = T$. Then

$$J_1 = \Delta S^2\, \overline{B^2}\, G^2(T) = \Delta S^2\, \overline{B^2} \left(\sum_{j=1}^{N} g_j \right)^2, \tag{4}$$

where we used the equality $G(T) = \sum_{j=1}^{N} g_j$. Thus, J_1 [Eq. (4)] contains N^2 terms, which are roughly of the same order. By comparison, for N measurements during time T, J_N in Eq. (3) contains N terms, which are a subset of the terms in Eq. (4), implying that $J_N/J_1 \sim 1/N$.

Hence, the slowdown of the system state decay under N stochastic system-bath coupling events that are interrupted by N projections on the initial state is similar to the well-known QZE scaling in the case of constant coupling [27].

The crucial insight transpiring from Eqs. (3) and (4) is that the decay of the system state in the stochastic QZE regime [65] depends on the sum of the *squared random couplings* g_j^2, as opposed to its dependence on the sum of g_j in $G(T)$ if the decay is measured at the end of the evolution during T. Hence, *a novel, unfamiliar role of projective measurements in the QZE regime*, beyond protecting the system state from decoherence, is revealed by this analysis: their ability to provide *information on the distribution of random, microscopic decoherence events* induced by the coupling of the system to the bath.

B. Continuous-variable noise unraveling by polarization probe measurements

We will now show that these results allow the unraveling of noise events that affect the photon polarization qubit, considered as a probe system coupled to a bath realized by a transverse spatial degree of freedom (DOF) of the photon. Namely, the photonic qubit propagates through a noisy channel in which decoherence occurs via coupling of the qubit with a spatial, continuous variable of the photon, acting as the bath. The propagation is a sequence of steps, each associated with a noise event; in the jth step, the coupling of the qubit with the continuous DOF is realized by the coupling of the polarization to the transverse position x of the photon, z being the propagation axis, with strength randomly changing at each step.

Specifically, the photonic qubit is dephased in the basis $\{|H\rangle, |V\rangle\}$, with H and V denoting the horizontal and vertical polarizations, respectively. The decoherence manifests itself as a spatial mismatch between the H and V polarization components: H polarization is (slightly) spatially shifted along the x axis by the unitary operator $U_j = \exp(ig_j P_x \otimes \Pi_H)$, where P_x denotes the transverse momentum along the x direction and $\Pi_H = |H\rangle\langle H|$.

In the general system-bath notation, $S = \Pi_H$ and $B = P_x$. The initial joint state of the qubit and the bath is

$$|\Psi_{\text{in}}\rangle = |\psi_\theta\rangle \otimes |f_x\rangle, \quad |\psi_\theta\rangle = \cos(\theta)|H\rangle + \sin(\theta)|V\rangle, \tag{5}$$

where $|f_x\rangle$ corresponds to the Gaussian wave packet

$$f(x) = \langle x|f_x\rangle = \frac{1}{(2\pi\sigma^2)^{1/4}} \exp\left(-\frac{x^2}{4\sigma^2}\right).$$

For the states in Eq. (5),

$$\Delta S^2 = \sin^2(\theta)\cos^2(\theta), \quad \overline{B^2} = \frac{1}{2\sigma^2}. \tag{6}$$

Since, in general, the bath state changes after each measurement, the decay parameter in Eq. (3) is now given by

$$J_N = \sin^2(\theta)\cos^2(\theta) \sum_{j=1}^{N} g_j^2 \overline{B^2}_j. \tag{7}$$

Here $\overline{B^2}_j$ is calculated for the spatial DOF wave packet evolving between the $(j-1)$th and jth measurements, whereas $\overline{B^2}_1 = \overline{B^2}$. According to Eq. (6), $\overline{B^2}$ is inversely proportional to the square of the wave packet width. Given that $B^2 = P_x^2$ applies the second derivative (with respect to x) to the wave packet, $\overline{B^2}_j$ generally decreases with the wave packet broadening. In our case, the wave packet evolution consists in its splitting into different subpackets which recede from each other, resulting, as long as the distance between the subpackets is less than their widths, in a broadening of the wave packet. Therefore, the quantities $\overline{B^2}_j$ in Eq. (7) are expected to decrease with j, causing a decrease of the decay parameter J_n, *in addition to the QZE*.

In our scenario, the quantum channel hosts N noise events, each characterized by a coupling strength randomly chosen from a finite set of values, $g_j \in \{G_1, \ldots, G_D\}$, with the probability p_k of the G_k noise event being independent of the order of the events. For example, in our proof-of-principle implementation, we have $N = 6$ and $D = 5$. In such a channel, the probability of observing $\{n_1, \ldots, n_D\}$ events of the type $\{G_1, \ldots, G_D\}$ is given by the multinomial distribution $M(n_1, \ldots, n_D) = \frac{N!}{n_1! \cdots n_D!} \prod_{k=1}^{D} p_k^{n_k}$, where $\sum_{k=1}^{D} n_k = N$ and $\sum_{k=1}^{D} p_k = 1$.

The corresponding (non-normalized) output state is

$$|\Psi_{\text{out}}\rangle = \Pi_\theta U_N \cdots \Pi_\theta U_1 |\Psi_{\text{in}}\rangle = |\psi_\theta\rangle \otimes \prod_{j=1}^{N} B_j |f_x\rangle, \tag{8}$$

where $\Pi_\theta = |\psi_\theta\rangle\langle\psi_\theta|$ and $B_j \equiv \cos^2(\theta)e^{ig_j P_x} + \sin^2(\theta)\mathbb{I}_d$, with $\mathbb{I}_d$ being the identity operator in the Hilbert space of the spatial DOF.

Since the B_j operators commute with each other, we can have

$$\prod_{j=1}^{N} B_j = \prod_{k=1}^{D} (\cos^2(\theta)e^{iG_k P_x} + \sin^2(\theta)\mathbb{I}_d)^{n_k},$$

highlighting how the spatial profile of $|\Psi_{\text{out}}\rangle$ depends only on the values of G_k and their multiplicity, not on their ordering. Hence, the probability of finding the photon in a specific position x_0 at the output of the quantum channel is

$$\mathcal{P}_N(x_0, \{n_k\}) = \frac{\left| \langle x_0| \prod_{k=1}^{D} B_k^{n_k} |f_x\rangle \right|^2}{\int dx' \left| \langle x'| \prod_{k=1}^{D} B_k^{n_k} |f_x\rangle \right|^2}. \tag{9}$$

Since we are interested in the estimation of the probability set $\{p_k\}$, we need to quantify the numbers $\{n_k\}$ of the decoherence events $\{G_k\}$. This is achieved by minimizing, for any position x, the statistical square distance

$$\Delta\mathcal{P}(\{n_k\}_c) \equiv \int dx\, [\mathcal{P}_N^{\text{exp}}(x) - \mathcal{P}_N(x, \{n_k\}_c)]^2,$$

with $\mathcal{P}_N^{\text{exp}}(x)$ being the distribution experimentally measured at the output of the quantum channel and $\mathcal{P}_N(x, \{n_k\}_c)$ the theoretical one given by the set $\{n_k\}_c$, with the integer index $c \in \left[1, \binom{D+N-1}{N}\right]$ labeling the theoretical distributions. The reconstructed set $\{n_k\}_R$ of the multiplicities of decoherence events is estimated as

$$\{n_k\}_R = \arg\min_c \Delta\mathcal{P}(\{n_k\}_c), \tag{10}$$

yielding the probabilities $\{p_k\}_R$, with $p_k = n_k/N$. To reduce the uncertainty on the estimated p_k values, one can repeat this procedure L times, thus obtaining each p_k as $p_k = \sum_{\ell=1}^{L} p_k^{(\ell)}/L$.

III. THE EXPERIMENT

In our setup, Alice exploits (Fig. 1) a laser source at 700 nm attenuated down to the single-photon level, and arbitrarily chooses as initial polarization state $|\psi_\theta\rangle = (|H\rangle + |V\rangle)/\sqrt{2} \equiv |+\rangle$. Then, a series of $N = 6$ decoherence-protection steps (with intensity chosen among the set $\{G_k\} = \{0, g, 2g, 3g, 4g\}$, with g being the minimum noise intensity) is implemented, each composed of a pair of birefringent crystals (BCs) followed by a polarizing beam splitter (PBS, used as a polarizer) and a half-wave plate (HWP).

In each pair of birefringent crystals, the first crystal (with optical axis cut at 45° with respect to the photon propagation direction) shifts the horizontal polarization, as compared to the vertical one, in the transverse direction x. The shift depends on the crystal thickness, and is

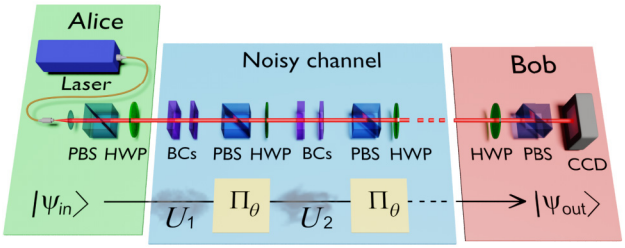

FIG. 1. Experimental setup and corresponding quantum operations. For the sake of simplicity, only two of the six noise events occurring in the quantum channel of our experimental realization are shown (see main text for abbreviations and more details).

associated to G_k. The second crystal (with optical axis at 90°) compensates for the temporal walk-off and phase mismatch between the H and V polarizations introduced by the previous crystal. Then, the PBS projects the photon onto its initial polarization state, thus inducing the QZE that protects the photon from decoherence. The HWP is used during the system initialization and optimization procedure, to verify the temporal walk-off and phase optimal compensation and carefully characterize the G_k noise intensity value induced by each pair (for which the $|H\rangle$ and $|V\rangle$ polarization eigenstates are needed).

At each step, we randomly choose among $D = 5$ different crystal thicknesses corresponding to the set $\{G_k\} = (0, g, 2g, 3g, 4g)$, with g being the minimum nonzero spatial displacement induced between the H and V polarization components. Finally, to prove the robustness of our technique even at extremely faint light regimes, at the end of the N decoherence-protection steps Bob detects the photons by means of a single-photon-sensitive electron-multiplied CCD camera with 1024×1024 pixels of size $13 \times 13\ \mu\text{m}^2$ (eventually projecting them onto Alice's initial polarization state by means of an HWP followed by a PBS), providing the final spatial distribution of the photons $f_{\text{out}}(x)$.

In principle, the setup in Fig. 1 allows the estimation of any set $\{n_k\}$ by means of Eq. (10). However, the minimization in Eq. (10) is very challenging, since it requires an extremely precise measurement of the whole probability distribution profile, which is especially hard to achieve for the distribution tails. Thus, in order to have a robust and reliable sensing procedure, we compare, instead of the

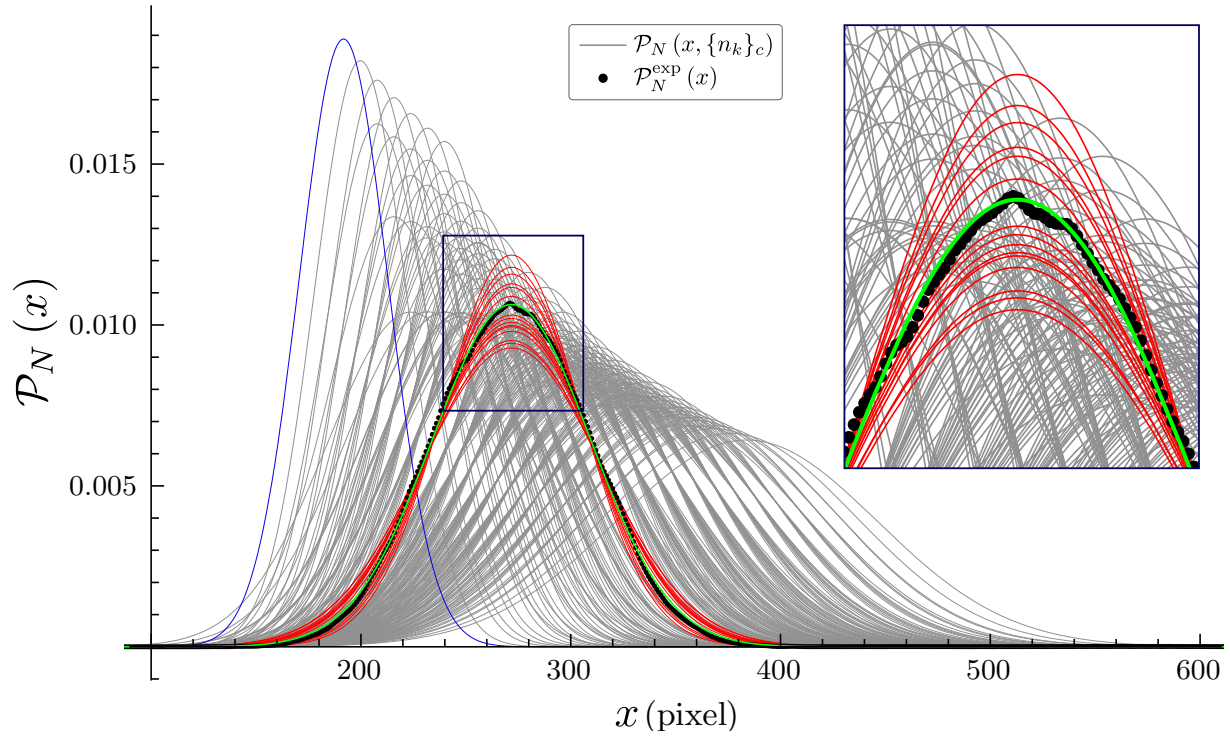

FIG. 2. Experimental estimation of $\{n_k\}_R$. The measured spatial distribution $\mathcal{P}_N^{\text{exp}}(x)$ is represented by the black dots, in very good agreement with the one given by the reconstructed set $\{n_k\}_R$ (green curve). The red curves correspond to the subset of probability configurations giving spatial distributions with the same average position and different standard deviations, whereas the gray curves are the distributions due to the remaining possible probability configurations. The inset shows an enlargement of the distribution peak region, allowing one to appreciate the correct discrimination performed within the subset of compatible noise configurations. Finally, the blue curve on the left, corresponding to the case of $N = 6$ null ($g = 0$) noise events, represents the initial spatial distribution of the photons.

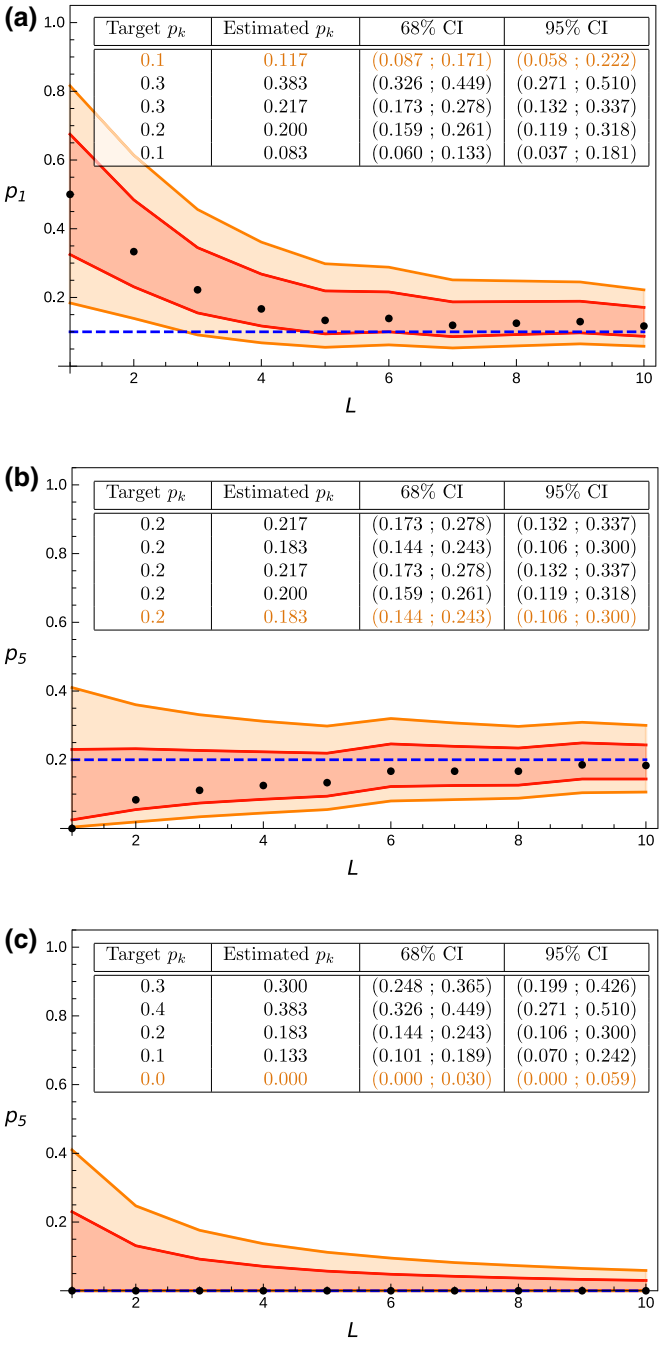

FIG. 3. Results obtained considering three different noise probability distribution sets, respectively, $\{p_k\} = (0.1, 0.3, 0.3, 0.2, 0.1)$ for panel (a), $\{p_k\} = (0.2, 0.2, 0.2, 0.2, 0.2)$ for panel (b), and $\{p_k\} = (0.3, 0.4, 0.2, 0.1, 0.0)$ for panel (c). The inset tables report the reconstructed noise probability distribution $\{p_k\}_R$ for a chosen set $\{p_k\}$, together with the 68% and 95% CIs on the estimated values after six steps. As an example, the graphs show, for each set, the behaviour of a particular p_k estimation (indicated in orange in the table) versus the number L of procedure realizations. The blue dashed lines represent the theoretical p_k value, while the black dots are the estimated values. The red and orange areas correspond, respectively, to the 68% and 95% CIs on the reconstructed p_k values.

entire distributions, only some of their moments:

$$E_c(x^i) = \int dx\, x^i \mathcal{P}_N(x, \{n_k\}_c),$$
$$E_{\exp}(x^i) = \int dx\, x^i \mathcal{P}_N^{\exp}(x). \tag{11}$$

Here, $E_c(x^i)$ and $E_{exp}(x^i)$ are, respectively, the ith moment of the theoretical distribution due to the set $\{n_k\}_c$ and the one extracted from the experimental spatial distribution $\mathcal{P}_N^{\exp}(x)$. In our case, we demonstrate that, thanks to our optimization approach, the first two moments suffice for faithfully extracting the $\{n_k\}_R$ set.

One can estimate the total amount of decoherence in the quantum channel by measuring the average position of $\mathcal{P}_N^{\exp}(x)$ both with and without exploiting the QZE, but this information is not enough to reconstruct the set $\{n_k\}_R$. To do this, we start from a subset of the possible configurations that correspond to the estimated average position $E_{\exp}(x)$, and apply the minimization on the second-order moment difference $\Delta E_c(x^2) \equiv E_{\exp}(x^2) - E_c(x^2)$. As a result, we obtain $\{n_k\}_R \simeq \arg\min_c(\Delta E_c(\Delta x^2))^2$ with $\Delta x \equiv x - E_{\exp}(x)$.

IV. RESULTS

In Fig. 2 we present our results for a particular realization of the quantum channel noise distribution, corresponding to the crystal set $\{n_k\} = (2, 0, 2, 2, 0)$. The experimental spatial distribution (black dots) is in very good agreement with the theoretical behavior (green curve) expected for the set $(2, 0, 2, 2, 0)$, correctly estimated by our sensing procedure. The theoretical survival probability of the original polarization state after $N = 6$ decoherence steps would be 0.50 without protection, but it reaches 0.58 when we apply the noise sensing technique that protects the state. In our experiment, this noise sensing technique yields a survival probability of 0.47 ± 0.01, but after subtracting the optical losses due to the $N = 6$ PBSs, whose total transmissivity amounts to 0.84 ± 0.03, we obtain a survival probability of 0.56 ± 0.03, in agreement with the theoretical prediction. This proves that we can sense the noise affecting the quantum channel while losing fewer probes in it, because of their higher survival probability granted by our technique.

In order to test the robustness and versatility of our technique, we apply it to three different noise event distributions (see Fig. 3). Then, to demonstrate the reduction of the uncertainty on the estimated p_k values for an increasing number of trials L, we collect data for $L = 10$ randomized crystal sets $\{n_k\}$ for each chosen $\{p_k\}$. Specifically, for each of the chosen noise distributions, n_k is randomly sampled with probability p_k for each $k = 1, \ldots, D$. Furthermore, we estimate a confidence interval (CI) for each extracted $\{p_k\}_R$ by exploiting the Beta distribution, which considers two

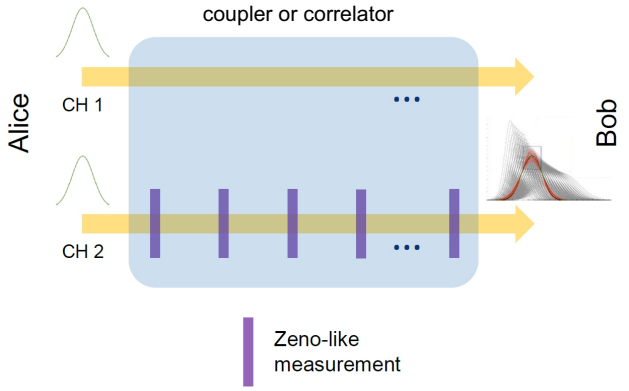

FIG. 4. Diagnostics of microscopic decoherence events, by pairing the communication channel (CH 1) with an identical auxiliary channel (CH 2) hosting similar photonic qubits (like, for example, two adjacent deployed optical fibers [68]). Thanks to the coupler or correlator of the two channels, they are affected by the same microscopic decoherence events. While in CH 1 the qubits propagate freely, in CH 2 the auxiliary qubits undergo multiple Zeno-like projective polarization measurements, allowing one to reconstruct the decoherence events in both channels and statistically correct their effect on the qubits exiting CH 1.

different coverage factors associated to the 68% and 95% CIs, respectively.

The results are presented in the tables reported as insets in Fig. 3, which correspond to the experimentally investigated $\{p_k\}$ sets. The estimated probabilities converge to the theoretical ones, within the 95% CI, even after only $L = 10$ realizations. In addition, in Fig. 3 we show, for each case, the typical behavior of the p_k estimation results as a function of the number L of the procedure realizations. In each plot, the theoretical target probability is represented by a blue dashed line, while the estimated values obtained for each L are shown by the black dots. The experimentally extracted $\{p_k\}$ sets are in good agreement with the theoretical expectations in all the three cases considered, with most of the expected p_k values falling within the 68% CI on the corresponding reconstructed value.

Application to depolarizing channels

Beyond the demonstration of this new fundamental concept, we point out its potentialities for novel diagnostics and control of noisy, depolarizing communication channels. To give an example (see Fig. 4), we envisage two identical channels, a communication channel (CH 1) and an auxiliary one (CH 2), which are coupled or correlated in some degree of freedom (like, for example, two adjacent deployed optical fibers [68]). Both channels are subject to the same decoherence (e.g., due to birefringence fluctuations in optical fibers [69]). The photonic qubits propagating in CH 1 are accompanied by auxiliary, frequently measured photonic qubits in CH 2, a scenario that could be obtained by diverting a small part of the signal in the communication channel to the auxiliary one. Because the qubits in the two channels share the same decoherence, frequent measurements of this diverted part in the auxiliary channel can sample the important moments of the noise distribution as per Eq. (11). This sampled information may be used in a feedback scheme to partly undo the deleterious effects of decoherence [27,29] on the main (unmeasured) part of the signal.

V. CONCLUSIONS

In this paper we have proposed and demonstrated, both theoretically and experimentally, a novel noise sensing technique for unraveling, i.e., estimating, the statistics of stochastic decoherence events affecting a noisy channel. Besides protection from decoherence of the (known) initial state of the qubit, QZE is shown to allow extraction of information about the statistics of the decoherence source affecting the channel upon detecting the photon only at the end of the channel. Our technique is enabled by attributing different functionalities to distinct degrees of freedom of the employed quantum particles (here, photons), allowing them to serve both as quantum carriers and as quantum sensors. This unique microscopic, protected information acquired by QZE and the ensuing correction may be viewed as the next generation of noise sensing and correcting schemes, as compared to a recent scheme [68] where phase fluctuations due to vibrations in a fiber are compensated by an auxiliary channel (yet without discriminating the decoherence events or protecting against them as we propose).

The proposed sensing technique has been experimentally demonstrated on a quantum optical setup, and has provided us with accurate results in each tested sequence of external decoherence events. Since our technique has been proven to be robust even at the single-photon level, it can be applied even in extremely faint-light scenarios like those involving highly photosensitive biosamples (e.g., the ocular retina). These samples are impossible to sense by traditional interferometric techniques, because the minimum illumination level needed for obtaining reliable results would already be strong enough to alter the sample [70–73]. Although a detailed description of the possible applications lies beyond the scope of this paper, this technique might be highly beneficial for the study of faint-light polarization effects in diverse biochemical and physical systems, such as cholesterol birefringence fluctuations in biological fluids for disease and defect diagnostics [74–76], or protein structure characterization by chirality [77].

Our results open the way to a new generation of noise diagnostic tools, allowing the monitoring of microscopic noise events by frequent measurements and eventually correcting for them. Future extensions of our approach may

concern quantum communication, e.g., for mitigating photon leakage from a channel by frequent perturbations [78], and eventually for the hampering of photon entanglement distribution by decoherence [69,79,80] and its mitigation by measurements [81,82].

ACKNOWLEDGMENTS

This work was financially supported by the European Union's Horizon 2020 Research and Innovation Programme under Grant Agreement No. 101113901 (Qu-Test) and FET-OPEN Grant Agreement No. 828946 (PATHOS). This work was also funded by the project QuaFuPhy (call "Trapezio" of Fondazione San Paolo) and by the projects EMPIR 19NRM06 METISQ and 20IND05 QADeT. These last two projects received funding by the EMPIR program cofinanced by the Participating States and from the European Union Horizon 2020 Research and Innovation Programme. G.K. acknowledges support from DFG (FOR 2724) and QUANTERA (PACE-IN).

The work was devised by G.K., F.C., M.Gen. and I.P.D., with the help of S.V., A.A., F.P., M.Gram and S.G. Theoretical framework was provided by G.K., A.K., F.C., I.P.D. and S.G. The experiment and the data analysis were run by S.V. and L.T.K. (principal investigators), under the supervision of A.A., F.P., I.P.D. and M.Gen. (responsible of the laboratories). The manuscript was written with inputs from all the authors.

[1] B. Chernobrod and G. Berman, Spin microscope based on optically detected magnetic resonance, J. Appl. Phys. **97**, 014903 (2005).

[2] J. Taylor, P. Cappellaro, L. Childress, L. Jiang, D. Budker, P. Hemmer, A. Yacoby, R. Walsworth, and M. D. Lukin, High-sensitivity diamond magnetometer with nanoscale resolution, Nat. Phys. **4**, 810 (2008).

[3] J. Maze *et al.*, Nanoscale magnetic sensing with an individual electronic spin in diamond, Nature **455**, 644 (2008).

[4] G. Balasubramanian *et al.*, Nanoscale imaging magnetometry with diamond spins under ambient conditions, Nature **455**, 648 (2008).

[5] R. Maiwald, D. Leibfried, J. Britton, J. C. Bergquist, L. Gerd, and D. J. Wineland, Stylus ion trap for enhanced access and sensing, Nat. Phys. **5**, 551 (2009).

[6] J. Bylander, S. Gustavsson, F. Yan, F. Yoshihara, K. Harrabi, G. Fitch, D. G. Cory, Y. Nakamura, J.-S. Tsai, and W. D. Oliver, Noise spectroscopy through dynamical decoupling with a superconducting flux qubit, Nat. Phys. **7**, 565 (2011).

[7] R. Kohlhaas, A. Bertoldi, E. Cantin, A. Aspect, A. Landragin, and P. Bouyer, Phase Locking a Clock Oscillator to a Coherent Atomic Ensemble, Phys. Rev. X **5**, 021011 (2015).

[8] C. L. Degen, F. Reinhard, and P. Cappellaro, Quantum sensing, Rev. Mod. Phys. **89**, 035002 (2017).

[9] M. Schioppo *et al.*, Ultrastable optical clock with two cold-atom ensembles, Nat. Photon. **11**, 48 (2017).

[10] F. Reiter, A. Sørensen, P. Zoller, and C. Muschik, Dissipative quantum error correction and application to quantum sensing with trapped ions, Nat. Commun. **8**, 1822 (2017).

[11] V. Frey, S. Mavadia, L. Norris, W. de Ferranti, D. Lucarelli, L. Viola, and M. Biercuk, Application of optimal band-limited control protocols to quantum noise sensing, Nat. Commun. **8**, 2189 (2017).

[12] L. Pezzè, A. Smerzi, M. K. Oberthaler, R. Schmied, and P. Treutlein, Quantum metrology with nonclassical states of atomic ensembles, Rev. Mod. Phys. **90**, 035005 (2018).

[13] S. Hernández-Gómez, F. Poggiali, P. Cappellaro, and N. Fabbri, Noise spectroscopy of a quantum-classical environment with a diamond qubit, Phys. Rev. B **98**, 214307 (2018).

[14] Y. Sung *et al.*, Non-Gaussian noise spectroscopy with a superconducting qubit sensor, Nat. Commun. **10**, 1 (2019).

[15] K. C. McCormick, J. Keller, S. C. Burd, D. J. Wineland, A. C. Wilson, and D. Leibfried, Quantum-enhanced sensing of a single-ion mechanical oscillator, Nature **572**, 86 (2019).

[16] J. F. Barry, J. M. Schloss, E. Bauch, M. J. Turner, C. A. Hart, L. M. Pham, and R. L. Walsworth, Sensitivity optimization for NV-diamond magnetometry, Rev. Mod. Phys. **92**, 015004 (2020).

[17] G. Petrini, E. Moreva, E. Bernardi, P. Traina, G. Tomagra, V. Carabelli, I. P. Degiovanni, and M. Genovese, Is a quantum biosensing revolution approaching? Perspectives in NV-assisted current and thermal biosensing in living cells, Adv. Quantum Technol. **3**, 2000066 (2020).

[18] G. Petrini *et al.*, Nanodiamond-quantum sensors reveal temperature variation associated to hippocampal neurons firing, Adv. Sci. **9**, 2202014 (2022),

[19] G. Palma, K.-A. Suominen, and A. Ekert, Quantum computers and dissipation, Proc. R. Soc. London Ser. A **529**, 567 (1996).

[20] C. Gardiner and P. Zoller, *Quantum Noise* (Springer, Berlin, 2000).

[21] H.-P. Breuer and F. Petruccione, *The Theory of Open Quantum Systems* (Oxford University Press, Oxford, 2002).

[22] F. Benatti and R. Floreanini, Open quantum dynamics: Complete positivity and entanglement, Int. J. Mod. Phys. **B19**, 3063 (2005).

[23] K. Khodjasteh, D. A. Lidar, and L. Viola, Arbitrarily Accurate Dynamical Control in Open Quantum Systems, Phys. Rev. Lett. **104**, 090501 (2010).

[24] F. Caruso, V. Giovannetti, C. Lupo, and S. Mancini, Quantum channels and memory effects, Rev. Mod. Phys. **86**, 1203 (2014).

[25] C. Addis, E.-M. Laine, C. Gneiting, and S. Maniscalco, Problem of coherent control in non-Markovian open quantum systems, Phys. Rev. A **94**, 052117 (2016).

[26] M. A. C. Rossi, C. Foti, A. Cuccoli, J. Trapani, P. Verrucchi, and M. G. A. Paris, Effective description of the short-time dynamics in open quantum systems, Phys. Rev. A **96**, 032116 (2017).

[27] G. Kurizki and A. G. Kofman, *Thermodynamics and Control of Open Quantum Systems* (Cambridge University Press, Cambridge, 2022).

[28] A. G. Kofman and G. Kurizki, Unified Theory of Dynamically Suppressed Qubit Decoherence in Thermal Baths, Phys. Rev. Lett. **93**, 130406 (2004).
[29] H. M. Wiseman and G. J. Milburn, *Quantum Measurement and Control* (Cambridge University Press, Cambridge, 2009).
[30] C. Brif, R. Chakrabarti, and H. Rabitz, Control of quantum phenomena: Past, present and future, New J. Phys. **12**, 075008 (2010).
[31] P. Zanardi and M. Rasetti, Noiseless Quantum Codes, Phys. Rev. Lett. **79**, 3306 (1997).
[32] D. A. Lidar, I. L. Chuang, and K. B. Whaley, Decoherence-Free Subspaces for Quantum Computation, Phys. Rev. Lett. **81**, 2594 (1998).
[33] P. Kwait, A. Berglund, J. Altepeter, and A. White, Experimental verification of decoherence-free subspaces, Science **290**, 498 (2000).
[34] J. Dowling and G. Milburn, Quantum technology: The second quantum revolution, Philos. Trans. Royal Soc. A **361**, 1655 (2003).
[35] J. O'Brien, A. Furusawa, and J. Vučković, Photonic quantum technologies, Nat. Photon. **3**, 687 (2009).
[36] G. Kurizki, P. Bertet, Y. Kubo, K. Mølmer, D. Petrosyan, P. Rabl, and J. Schmiedmayer, Quantum technologies with hybrid systems, Proc. Natl. Acad. Sci. **112**, 3866 (2015).
[37] A. Streltsov, G. Adesso, and M. B. Plenio, Colloquium: Quantum coherence as a resource, Rev. Mod. Phys. **89**, 041003 (2017).
[38] M. S. Safronova, D. Budker, D. DeMille, D. F. J. Kimball, A. Derevianko, and C. W. Clark, Search for new physics with atoms and molecules, Rev. Mod. Phys. **90**, 025008 (2018).
[39] J. Wang, F. Sciarrino, A. Laing, and M. Thompson, Integrated photonic quantum technologies, Nat. Photon. **14**, 273 (2020).
[40] C. Adams, J. Pritchard, and J. Shaffer, Rydberg atom quantum technologies, J. Phys. B: At. Mol. Opt. **53**, 012002 (2020).
[41] M. Genovese, Experimental quantum enhanced optical interferometry, AVS Quantum Sci. **3**, 044702 (2021).
[42] R. Horodecki, Quantum information, Acta Phys. Pol. A **139**, 197 (2021).
[43] K. Yamamoto, S. Endo, H. Hakoshima, Y. Matsuzaki, and Y. Tokunaga, Error-Mitigated Quantum Metrology via Virtual Purification, Phys. Rev. Lett. **129**, 250503 (2022).
[44] G. A. Álvarez and D. Suter, Measuring the Spectrum of Colored Noise by Dynamical Decoupling, Phys. Rev. Lett. **107**, 230501 (2011).
[45] T. Yuge, S. Sasaki, and Y. Hirayama, Measurement of the Noise Spectrum Using a Multiple-Pulse Sequence, Phys. Rev. Lett. **107**, 170504 (2011).
[46] G. A. Paz-Silva and L. Viola, General Transfer-Function Approach to Noise Filtering in Open-Loop Quantum Control, Phys. Rev. Lett. **113**, 250501 (2014).
[47] A. Zwick, G. A. Álvarez, and G. Kurizki, Maximizing information on the environment by dynamically controlled qubit probes, Phys. Rev. Appl. **5**, 014007 (2016).
[48] L. M. Norris, G. A. Paz-Silva, and L. Viola, Qubit Noise Spectroscopy for Non-Gaussian Dephasing Environments, Phys. Rev. Lett. **116**, 150503 (2016).
[49] M. M. Müller, S. Gherardini, and F. Caruso, Stochastic quantum Zeno-based detection of noise correlations, Sci. Rep. **6**, 38650 (2016).
[50] P. Szańkowski, G. Ramon, J. Krzywda, D. Kwiatkowski, and Ł. Cywiński, Environmental noise spectroscopy with qubits subjected to dynamical decoupling, J. Phys.: Condens. Matter **29**, 333001 (2017).
[51] M. M. Müller, S. Gherardini, and F. Caruso, Noise-robust quantum sensing via optimal multi-probe spectroscopy, Sci. Rep. **8**, 1 (2018).
[52] J. Krzywda, P. Szańkowski, and Ł. Cywiński, The dynamical-decoupling-based spatiotemporal noise spectroscopy, New J. Phys. **21**, 043034 (2019).
[53] H.-V. Do, C. Lovecchio, I. Mastroserio, N. Fabbri, F. S. Cataliotti, S. Gherardini, M. M. Müller, N. Dalla Pozza, and F. Caruso, Experimental proof of quantum Zeno-assisted noise sensing, New J. Phys. **21**, 113056 (2019).
[54] F. Sakuldee and L. Cywiński, Relationship between subjecting the qubit to dynamical decoupling and to a sequence of projective measurements, Phys. Rev. A **101**, 042329 (2020).
[55] M. M. Müller, S. Gherardini, N. Dalla Pozza, and F. Caruso, Noise sensing via stochastic quantum Zeno, Phys. Lett. A **384**, 126244 (2020).
[56] B. Misra and E. Sudarshan, The Zeno's paradox in quantum theory, J. Math. Phys. **18**, 756 (1977).
[57] W. M. Itano, D. J. Heinzen, J. J. Bollinger, and D. J. Wineland, Quantum Zeno effect, Phys. Rev. A **41**, 2295 (1990).
[58] A. G. Kofman and G. Kurizki, Quantum Zeno effect on atomic excitation decay in resonators, Phys. Rev. A **54**, R3750 (1996).
[59] D. Home and M. Whitaker, A conceptual analysis of quantum Zeno; paradox, measurement, and experiment, Ann. Phys. (N.Y.) **258**, 237 (1997).
[60] P. Facchi and S. Pascazio, Quantum Zeno Subspaces, Phys. Rev. Lett. **89**, 080401 (2002).
[61] K. Koshino and A. Shimizu, Quantum Zeno effect by general measurements, Phys. Rep. **412**, 191 (2005).
[62] P. Facchi and S. Pascazio, Quantum Zeno dynamics: Mathematical and physical aspects, J. Phys. A: Math. Theor. **41**, 493001 (2008).
[63] F. Schäfer, I. Herrera, S. Cherukattil, C. Lovecchio, F. Cataliotti, F. Caruso, and A. Smerzi, Experimental realization of quantum Zeno dynamics, Nat. Commun. **5**, 3194 (2014).
[64] A. Signoles, A. Facon, D. Grosso, I. Dotsenko, S. Haroche, J.-M. Raimond, M. Brune, and S. Gleyzes, Confined quantum Zeno dynamics of a watched atomic arrow, Nat. Phys. **10**, 715 (2014).
[65] S. Gherardini, S. Gupta, F. S. Cataliotti, A. Smerzi, F. Caruso, and S. Ruffo, Stochastic quantum Zeno by large deviation theory, New J. Phys. **18**, 013048 (2016).
[66] X. Long *et al.*, Entanglement-Enhanced Quantum Metrology in Colored Noise by Quantum Zeno Effect, Phys. Rev. Lett. **129**, 070502 (2022).
[67] S. Virzì, A. Avella, F. Piacentini, M. Gramegna, T. Opatrný, A. G. Kofman, G. Kurizki, S. Gherardini, F. Caruso, I. P. Degiovanni, and M. Genovese, Quantum Zeno and Anti-Zeno Probes of Noise Correlations in Photon Polarization, Phys. Rev. Lett. **129**, 030401 (2022).

[68] C. Clivati, A. Tampellini, A. Mura, F. Levi, G. Marra, P. Galea, A. Xuereb, and D. Calonico, Optical frequency transfer over submarine fiber links, Optica **5**, 893 (2018).
[69] G. Gordon and G. Kurizki, How to maximize the capacity of general quantum noisy channels, Fortschritte der Physik **57**, 1071 (2009).
[70] K. R. Byrnes, X. Wu, R. W. Waynant, I. K. Ilev, and J. J. Anders, Low power laser irradiation alters gene expression of olfactory ensheathing cells in vitro, Lasers Surg. Med. **37**, 161 (2005).
[71] R. Lubart, R. Lavi, H. Friedmann, and S. Rochkind, Photochemistry and photobiology of light absorption by living cells, Photomed. Laser Surg. **24**, 179 (2006), pMID: 16706696.
[72] N. S. Da Silva and J. W. Potrich, Effect of GaAlAs laser irradiation on enzyme activity, Photomed. Laser Surg. **28**, 431 (2010).
[73] C. A. Casacio, L. S. Madsen, A. Terrasson, M. Waleed, K. Barnscheidt, B. Hage, M. A. Taylor, and W. P. Bowen, Quantum-enhanced nonlinear microscopy, Nature **594**, 201 (2021).
[74] M. M. Zakharova, V. A. Nasonova, A. F. Konstantinova, V. S. Chudakov, and R. V. Gaĭnutdinov, An investigation of the optical properties of cholesterol crystals in human synovial fluid, Crystallogr. Rep. **54**, 509 (2009).
[75] M. Kashiwagi, L. Liu, K. K. Chu, C.-H. Sun, A. Tanaka, J. A. Gardecki, and G. J. Tearney, Feasibility of the assessment of cholesterol crystals in human macrophages using micro optical coherence tomography, PLoS ONE **9**, 1 (2014).
[76] A. Gevorgyan, M. Z. Harutyunyan, G. K. Matinyan, K. B. Oganesyan, Y. V. Rostovtsev, G. Kurizki, and M. O. Scully, Absorption and emission in defective cholesteric liquid crystal cells, Laser Phys. Lett. **13**, 046002 (2016).
[77] L. Whitmore and B. A. Wallace, Protein secondary structure analyses from circular dichroism spectroscopy: Methods and reference databases, Biopolymers **89**, 392 (2008).
[78] L.-A. Wu, G. Kurizki, and P. Brumer, Master Equation and Control of an Open Quantum System with Leakage, Phys. Rev. Lett. **102**, 080405 (2009).
[79] C. Macchiavello and G. M. Palma, Entanglement-enhanced information transmission over a quantum channel with correlated noise, Phys. Rev. A **65**, 050301 (2002).
[80] V. Giovannetti, A dynamical model for quantum memory channels, J. Phys. A: Math. Gen. **38**, 10989 (2005).
[81] M. P. Almeida, F. de Melo, M. Hor-Meyll, A. Salles, S. P. Walborn, P. H. S. Ribeiro, and L. Davidovich, Environment-induced sudden death of entanglement, Science **316**, 579 (2007).
[82] Y. Wang *et al.*, Remote entanglement distribution in a quantum network via multinode indistinguishability of photons, Phys. Rev. A **106**, 032609 (2022).